Simulation of Interferometric SAR Response for Characterizing the Scattering Phase Center Statistics of Forest Canopies

Kamal Sarabandi, *Fellow, IEEE,* and Yi-Cheng Lin, *Member, IEEE*

***Abstract*—A coherent scattering model for tree canopies is employed in order to characterize the sensitivity of an interferometric SAR (INSAR) response to the physical parameters of forest stands. The concept of an equivalent scatterer for a collection of scatterers within a pixel, representing the vegetation particles of tree structures, is used for identifying the scattering phase center of the pixel whose height is measured by an INSAR. Combining the recently developed coherent scattering model for tree canopies and the INSAR Δk-radar-equivalence algorithm, accurate statistics of the scattering phase-center location of forest stands are obtained numerically for the first time. The scattering model is based on a Monte Carlo simulation of scattering from fractal-generated tree structures, and therefore is capable of preserving the absolute phase of the backscatter. The model can also account for coherent effects due to the relative position of individual scatterers and the inhomogeneous extinction experienced by a coherent wave propagating through the random collection of vegetation particles. The location of the scattering phase center and the correlation coefficient are computed using the Δk-radar equivalence simply by simulating the backscatter response at two slightly different frequencies. The model is successfully validated using the measured data acquired by JPL TOPSAR over a selected pine stand in Raco, MI. A sensitivity analysis is performed to characterize the response of coniferous and deciduous forest stands to a multifrequency and multipolarization INSAR in order to determine an optimum system configuration for remote sensing of forest parameters.**

***Index Terms*—Forest scattering, SAR interferometry, radar vegetation model.**

I. Introduction

ACCURATE estimation of gross forest parameters such as total vegetation biomass, total leaf-area index, and tree height in global scale has long been an important goal within the remote sensing community. Over the past two decades, much effort has been devoted to the development of scattering models [1]–[6] for understanding the interaction of electromagnetic waves with vegetation, and to the construction and development of advanced-imaging radars for acquiring test data and examining the feasibility of the remote sensing problem [7], [8]. In most practical situations, the number of vegetation parameters influencing the radar response usually exceeds the number of radar-observation parameters. For this reason, the application of a multifrequency and multipolarization radar system was proposed, and such a system was flown aboard the Space Shuttle Endeavor in April and October of 1994 [8]. Preliminary results indicate that the classification and retrieval of vegetation-biophysical parameters indeed require many simultaneous radar channels. However, free-flight of such systems is not practical due to the exorbitant power requirements.

Recent advancements in the field of radar interferometry have opened a new door to the radar remote sensing of vegetation. In addition to the backscattering coefficient, radar interferometers measure two additional quantities that contain target information [9]. These quantities are the correlation coefficient and the interferogram phase. To interpret these quantities and to characterize their dependency on the physical parameters of the target, a thorough understanding of the coherent interaction of electromagnetic waves with vegetation particles is required. The premise of this investigation with regard to retrieving vegetation parameters from INSAR data stems from the fact that the location of the scattering-phase center of a target is a strong function of the target structure. For example, the scattering-phase centers of nonvegetated terrain are located at or slightly below the surface, depending upon the wavelength and the dielectric properties of the surface media, whereas for vegetated terrain, these scattering phase centers lie at or above the surface, depending upon the wavelength of the SAR and the vegetation attributes. It also must be recognized that the vegetation cover adds noise in many interferometric SAR applications in which the vegetation itself is not the primary target, such as geological field mapping or surface-change monitoring. In these cases, it is also important to identify and characterize the effect of vegetation on the topographic information obtained from the interferometric SAR.

In recent years, some experimental and theoretical studies have been carried out to demonstrate the potential INSAR's in retrieving forest parameters. For example, in [10]–[12], experimental data using ERS-1 SAR repeat-pass and TOPSAR single-pass are employed to show the applications of SAR interferometry for classification of forest types and retrieval of tree heights. Also, theoretical models have been developed to establish relationships between the interferogram phase and correlation coefficient to the physical parameters of vegetation and the underlying soil surface [13]–[15]. Although these models give qualitative explanations for the measured data and provide a basic understanding of the problem, due to the oversimplified assumptions in the description of vegetation structure, they

Manuscript received April 2, 1997; revised October 13, 1998. This investigation was supported by NASA under Contract NAG5-4939.

The authors are with the Radiation Laboratory, Department of Electrical Engineering and Computer Science, University of Michigan, Ann Arbor, MI 48109-2122 USA (e-mail: saraband@eecs.umich.edu).

Publisher Item Identifier S 0196-2892(00)00022-X.

are not accurate enough for most practical applications. For example, the shape, size, number density, and orientation distributions of vegetation in forest stands are nonuniform along the vertical direction. The nonuniform distributions of physical parameters of vegetation particles (such as leaves and branches) give rise to inhomogeneous scattering and extinction, which significantly affects the correlation coefficient and the location of the vegetation-scattering phase center.

The purpose of this investigation is to develop a robust scattering model for forest canopies capable of predicting the response of INSAR's. Although there are a number of EM scattering models available for vegetation canopies [1]–[3], [5], [6] they are of little use with regard to INSAR applications due to their inability to predict the absolute phase of the scattered field. The absolute phase of the scattered field is the fundamental quantity from which the interferogram images are constructed. The proposed model described in Section II is basically composed of two recently developed algorithms: a fully coherent scattering model for tree canopies based on a Monte Carlo simulation of scattering from fractal-generated trees [16], and an extraction of the scattering-phase center based on a Δk-radar equivalence relationship with INSAR [13]. In Section III the validity of the model in predicting the backscatter coefficients and the location of the scattering phase center of forest canopies is demonstrated by comparing the simulated results with those measured by JPL TOPSAR [17]. Finally a sensitivity study is conducted to demonstrate the variations of the scattering phase center of a forest stand in terms of target parameters such as tree density, soil moisture, tree type, and ground tilt angle, as well as INSAR parameters such as polarization, frequency, and incidence angle.

In this section, an overview is given of the approaches that are employed to extract statistics of the scattering phase center of forest canopies. Three tasks must be undertaken for the calculation of the correlation coefficient and the location of the scattering phase center. These include: 1) accurate simulation of tree structures; 2) development of the scattering model; and 3) development of an algorithm for evaluation of the location of the scattering phase center.

Fig. 1. Photograph of a red pine stand (Stand 22) and the simulated tree structure using the fractal model.

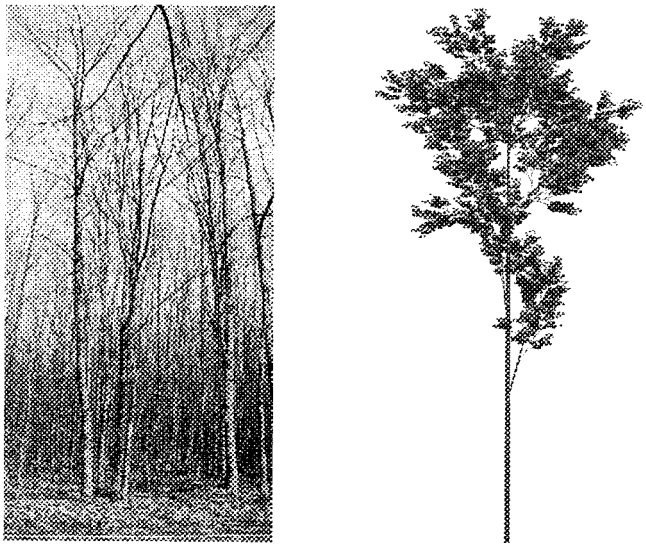

Fig. 2. Photograph of a red maple stand (Stand 31) and the simulated tree structure using the fractal model.

II. Model Description

A. Fractal Model

It will be shown that the location of the scattering phase center of a tree is a strong function of the tree structure. For an accurate estimation of the scattering phase center and the backscattering coefficients, the algorithm for generating desired tree structures must be capable of producing realistic tree structures and yet be as simple as possible. It has been shown that geometrical features of most botanical structures can be described by only a few parameters using fractal theory [18], [19]. A distinctive feature of fractal patterns is the self-similarity that is maintained throughout the derivation process. To generate fractal patterns, we use Lindenmayer systems [20], which are versatile tools for implementing the self-similarity throughout a so-called rewriting process. For a tree-like structure, some essential botanical features must be added to the fractal process, including branch tapering in length and cross section, leaf placement, and randomizing the fractal parameters according to some prescribed probability-density functions. The botanical features and the probability-density functions must be characterized according to *in situ* measurements of a given stand.

Although there are many computer graphics available for generating tree-like structures, most are not appropriate for the purpose of scientific modeling. At microwave frequencies, the radar return and its statistics strongly depend on tree structures, which necessitate the application of realistic models for generating accurate tree structures. Therefore, the final and most important step in the fractal model is to incorporate the information about the tree structure and its statistics obtained from the *in situ* measurements of the ground truth. Figs. 1 and 2 compare the simulated trees produced by the fractal model developed in this paper with the photographs of the actual forest stands. These simulated structures are generated according to *in situ* measurements collected from two test sites denoted by Stand 22 (red pine) and Stand 31 (red maple) in Raco, MI. The

fractal pine shown in Fig. 1(b) consists of 792 branch segments, 391 end-needle clusters, and 747 needle-covered stems. The fractal maple in Fig. 2(b) comprises 7494 branch segments and 14 818 leaves, consistent with the ground-truth data [16]. To visualize the generated three-dimensional (3-D) tree structure, the fractal model is equipped with a fast algorithm that displays the real-time projected tree image with arbitrary scaling and perspective view.

B. Scattering Model

In contrast to the existing scattering models for tree canopies, the coherent model used in this investigation is capable of preserving the absolute phase of the backscatter as well as the relative phases of individual scatterers, which gives rise to coherent effects. Once a tree structure is generated, the scattered field is computed by considering the tree structure as a cluster of scatterers composed of cylinders (trunks and branches) and disks/needles (leaves) with specified position, orientation, and size. The attenuation and phase shift due to the scattering and absorption losses of vegetation particles within the tree canopy are taken into account in the computation of the scattered field from individual particles. To the first order of scattering approximation, the backscatter from the entire tree is calculated from the coherent addition of the individual scattering terms. Hence, neglecting the multiple scattering among the scatterers, the total scattered field can be written as

$$\mathbf{E}^s = \frac{e^{ikr}}{r} \sum_{n=1}^{N} e^{i\phi_n} \mathbf{S}_n \cdot \mathbf{E}_o^i \tag{1}$$

where N is the total number of the scatterers, $\mathbf{S}_n$ is the individual scattering matrix of the nth scatterer, which may be a tree trunk [21] or a vegetation needle [22], and ϕ_n is the phase compensation accounting for the shifting of the phase reference from the local to the global phase reference. This is given by $\phi_n = k_0(\hat{k}_i - \hat{k}_s) \cdot \mathbf{r_n}$, where $\mathbf{r_n}$ is the position vector of the nth scatterer in the global-coordinate system.

In order to compute the scattering matrix of the nth particle $\mathbf{S}_n$, consider a single particle above a ground plane. Ignoring the multiple scattering between the scatterer and its mirror image, the scattering matrix is composed of four components:

1) direct component $\mathbf{S}_n^t$;
2) ground-scatterer component $\mathbf{S}_n^{tg}$;
3) scatterer-ground component $\mathbf{S}_n^{gt}$;
4) ground-scatterer ground component $\mathbf{S}_n^{gtg}$.

Therefore, the individual scattering matrix $\mathbf{S}_n$ can be written as

$$\mathbf{S}_n = \mathbf{S}_n^t + \mathbf{S}_n^{gt} + \mathbf{S}_n^{tg} + \mathbf{S}_n^{gtg} \tag{2}$$

$$\mathbf{S}_n^t = \mathbf{T}_n^i \cdot \mathbf{S}_n^o(-\hat{k}_i, \hat{k}_i) \cdot \mathbf{T}_n^i \tag{3}$$

where

$$\mathbf{S}_n^{gt} = e^{i\tau_n} \mathbf{T}^t \cdot \mathbf{R} \cdot \mathbf{T}_n^r \cdot \mathbf{S}_n^0(-\hat{k}_r, \hat{k}_i) \cdot \mathbf{T}_n^i \tag{4}$$

$$\mathbf{S}_n^{tg} = e^{i\tau_n} \mathbf{T}_n^i \cdot \mathbf{S}_n^0(-\hat{k}_i, \hat{k}_r) \cdot \mathbf{T}_n^r \cdot \mathbf{R} \cdot \mathbf{T}^t \tag{5}$$

$$\mathbf{S}_n^{gtg} = e^{i2\tau_n} \mathbf{T}^t \cdot \mathbf{R} \cdot \mathbf{T}_n^r \cdot \mathbf{S}_n^0(-\hat{k}_r, \hat{k}_r) \cdot \mathbf{T}_n^r \cdot \mathbf{R} \cdot \mathbf{T}^t \tag{6}$$

with $\hat{k}_r = \hat{k}_i - 2\hat{n}_g(\hat{n}_g \cdot \hat{k}_i)$ and $\tau_n = 2k_0(\mathbf{r_n} \cdot \hat{n}_g)(\hat{n}_g \cdot \hat{k}_r)$. In the above expression, $\hat{n}_g$ is the unit vector normal to the ground plane, which in general is tilted with respect to the horizontal plane of the global-coordinate system. The optical length τ_n accounts for the extra path length experienced by the ground-scatterer or the scatterer-ground scattering components compared to the direct-scattering component. $\mathbf{S_n^0}$ is the scattering matrix of the nth scatterer isolated in free space. $\mathbf{R}$ is the reflection matrix of the ground plane, which includes the surface-reflection coefficient and the polarization transformation due to the tilted ground plane. $\mathbf{T}_n^i$ and $\mathbf{T}_n^r$ are transmissivity matrices accounting for the attenuation and phase change of the mean-field from the canopy top and the ground to the scatterer respectively, and $\mathbf{T}^t$ is the total canopy transmissivity (see Fig. 3).

A forest stand with a closed canopy can be regarded as a multilayered random medium, in which the properties of each layer can be characterized according to the particle distribution along the vertical extent of the forest canopy. The particle size, shape, position, and orientation distributions are obtained directly from the fractal model. A continuous multilayer random medium is not an accurate representation for the discontinuous canopies such as coniferous forest stands. In these cases, the mean field within the canopy is a function of both the vertical and horizontal positions, as shown in Fig. 4. The scattering model developed for this study has the ability to keep track of the attenuation and phase shift of the incident and reflected rays as they traverse the discontinuous canopies. This is accomplished by defining an envelope obtained from the fractal model for the tree canopy. Depending on the incidence angle, the incident or reflected rays may traverse the neighboring trees [23]. In the Monte Carlo simulation, the position of the neighboring trees is chosen randomly according to the tree density and plantation.

C. Algorithms for Evaluating the Location of the Scattering-Phase Center

As mentioned earlier, the overall objective of this investigation is to study the relationship between the phase and correlation coefficient of an INSAR interferogram and the physical parameters of a forest stand. An INSAR system measures the backscatter of a scene at two slightly different look angles, and the phase difference between the two backscattered fields is used to derive the elevation information. In a recent study [13], it has been established that similar information can be obtained by measuring the backscatter of the scene at two slightly different frequencies provided the look angle is known. For an INSAR system with known baseline distance (B) and angle α operating at frequency f_0, the frequency shift (Δf) of an equivalent Δk-radar is given by

$$\Delta f = \frac{f_0 B}{mr} \sin(\alpha - \theta) \tag{7}$$

where θ is the looking angle, $m = 1, 2$ for repeat-pass and two-antenna INSAR configurations, respectively, and r is the distance between the antenna and the scatterer. This equivalence relationship is specifically useful for numerical simulations and controlled experiments using stepped-frequency scatterometer systems. In Monte Carlo simulations, once the tree structure and

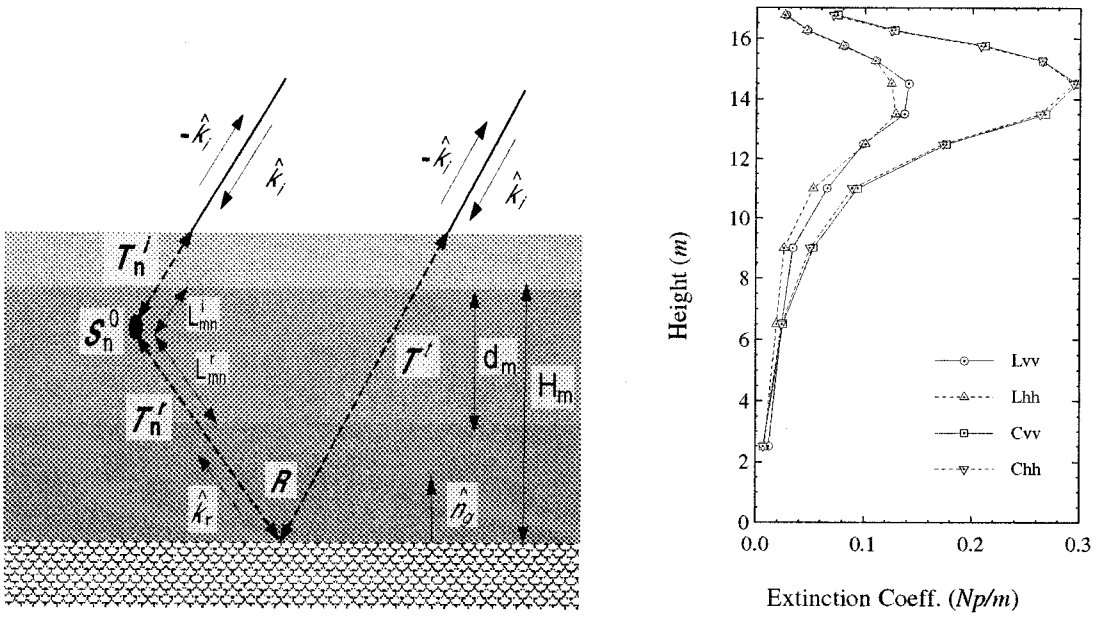

Fig. 3. (a) Propagation of a coherent wave in a continuous canopy and (b) an example of extinction profile calculated for Stand 31.

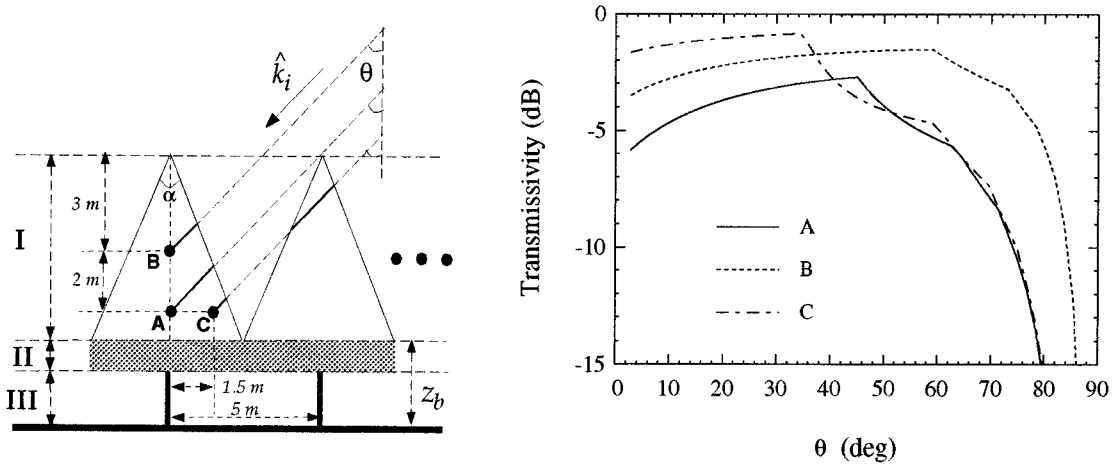

Fig. 4. Position dependence of the transmissivity for coniferous trees and the shadow effect caused by neighboring trees.

the scattering configuration are determined, the backscatter signals are calculated twice at two slightly different frequencies. The backscatter at $f_1 = f_0$ and $f_2 = f_0 + \Delta f$ are represented by E_1 and E_2, respectively, which are computed from

$$E_1 = \sum_{n=1}^{N} e^{2ik_0\hat{k}_i\cdot\mathbf{r_n}}\mathbf{S}_n(k_0)\cdot\mathbf{E}_o^i, \tag{8}$$

$$E_2 = \sum_{n=1}^{N} e^{2i(k_0+\Delta k)\hat{k}_i\cdot\mathbf{r_n}}\mathbf{S}_n(k_0+\Delta k)\cdot\mathbf{E}_o^i. \tag{9}$$

It is also shown that the height of the equivalent scatterer above the x–y plane of the global-coordinate system can be determined from

$$z_e = \frac{-\Delta\Phi}{2\Delta k\cos\theta} \tag{10}$$

where $\Delta k = 2\pi\Delta f/c$ and $\Delta\Phi = \angle(E_1^* E_2)$ represents the phase difference between E_1 and E_2. Note that the equivalent frequency shift for most practical INSAR configurations is only a small fraction of the center frequency ($\Delta f/f_0 < 0.1\%$) and therefore, the far-field amplitudes of individual isolated scatterers (S_n^0) do not change when the frequency is changed from f_0 to $f_0 + \Delta f$, that is, $S_n^0(k_0) \simeq S_n^0(k_0 + \Delta k)$. This approximation speeds up the Monte Carlo simulation without compromising the overall accuracy of scattering-phase center-height estimation.

For a random medium like a forest stand, the scattering-phase center-height (z_e) is a random variable whose statistics are of interest. Usually, the mean value and the second moment of this random variable are sought. Based on a rigorous statistical analysis [13], it is shown that the statistics of $\Delta\Phi$ can be obtained

from the frequency correlation function of the target by computing

$$\alpha e^{i\zeta} = \frac{\langle E_1^* E_2 \rangle}{\sqrt{\langle |E_1|^2 \rangle \langle |E_2|^2 \rangle}} \tag{11}$$

where α is the correlation coefficient, and ζ is the coherent phase difference. In (11), $\langle \cdot \rangle$ denotes the ensemble averaging, which is evaluated approximately using a sufficiently large number of realizations through the Monte Carlo simulation. When the backscatter statistics are Gaussian, α and ζ provide a complete description of the statistics of $\Delta\Phi$. The apparent height of the scattering phase center of a forest stand is proportional to ζ and can be obtained from

$$z_e = \frac{-\zeta}{2\Delta k \cos\theta}. \tag{12}$$

Note that ζ is not the statistical mean of $\Delta\Phi$, but rather the phase value at which the probability-density function of $\Delta\Phi$ assumes its maximum. In fact, using the mean value may result in a significant error for calculating the apparent height z_e. To demonstrate this, two cases may be considered. In one case, $\zeta = 0$, and in the other case $\zeta = 180°$. In both cases, the mean value of $\Delta\Phi$ is zero, whereas the apparent heights calculated from (12) are obviously different.

In order to develop some intuition about the scattering phase center and to examine the validity of the above equivalence algorithms, let us consider a simple case, in which the target is a single scatterer above a ground plane. Through this illustrative case, the relationship between the location of the scattering phase center and the scattering mechanisms can be demonstrated. Consider a dielectric cylinder of radius $a = 5$ cm, length $b = 3$ m, and dielectric constant $\epsilon_t = 22 + i10$, which is located at height $h = 6$ m above a ground plane having a complex permittivity $\epsilon_g = 9.7 + i1.6$. Suppose the target is illuminated by a plane wave whose direction of propagation is determined by the incident angles $\theta_i = 30°$, $\phi_i = 180°$, as shown in Fig. 5. As mentioned previously, the backscattered field is mainly composed of four scattering components with different path lengths. In general, it is quite difficult to characterize the location of the scattering phase center of a scatterer analytically when multipath scattering mechanisms are involved. However, in cases where a single scattering mechanism is dominant, it is found that the location of the scattering center is strongly dependent upon the path length of the dominant scattering component.

Here we illustrate this fact through an experimental study in which the orientation of the cylinder is properly arranged in four configurations, as shown in Fig. 5(a)–(d), such that the total backscatter is dominated by (a) S^t, (b) S^{gb}, (c) S^{gtg}, and (d) $S^t + S^{gb}$, respectively. Note that S^{gb} is the combination of the reciprocal pair S^{gt} and S^{tg}. The simulation results at f_0 =1.25 GHz are shown in Table I and include the scattering phase-center height normalized to the physical height z_e/h, the ratio of the amplitude of individual scattering components to the total backscattered field $|S^{(\cdot)}/S|$, and the overall radar cross section (RCS) of the target for each orientation configuration and for both polarizations. It is obvious from the results reported in Table I that in scattering configuration (a), where the backscatter is dominated by the direct component ($S^t/S = 0.99$), the location of the scattering phase center appears at the physical location of the scatterer above the ground ($z_e/h \simeq 1$). Similarly, in scattering configurations (b) and (c), where the backscatter is dominated by the single ground bounce component and the double ground bounce component, the locations of the scattering phase center appear on the ground surface and at the mirror-image point as shown in Fig. 5. In scattering configuration (d), the direct and the single ground bounce components of the backscatter are comparable in magnitude, and as shown in Table I, the location of the scattering phase center in this case appears at a point between the physical location of the scatterer and the ground surface. When the number of scatterers is large, the location of the scattering phase center is a convoluted function of physical locations of the constituent scatterers and the relative magnitudes and phases of the scattering components. Note that $|z_e/h|$ and $|S^{(\cdot)}/S|$ in Table I may exceed 1 since the total backscattered field S is the superposition of four scattering components that are not necessarily in phase.

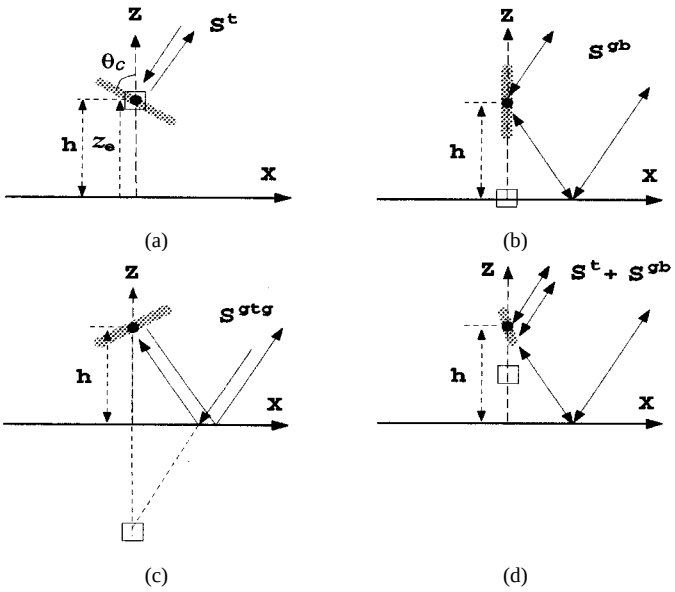

Fig. 5. Four configurations for a cylinder above a ground plane with orientation angles: (a) $\theta_c = 60°$, $\phi_c = 180°$, (b) $\theta_c = 0°$, $\phi_c = 0°$, (c) $\theta_c = 60°$, $\phi_c = 0°$, and (d) $\theta_c = 45°$, $\phi_c = 150°$ and their principal scattering mechanisms, respectively. The center of the scatterer is denoted by (•) and equivalent scattering phase center by (□).

TABLE I
NORMALIZED HEIGHT OF THE SCATTERING PHASE CENTER, THE NORMALIZED-SCATTERING COMPONENTS, AND THE RADAR CROSS SECTION FOR FOUR DIFFERENT SCATTERING CONFIGURATIONS, AS SHOWN IN FIG. 5.

Configuration	(a)		(b)		(c)		(d)	
Polarization	vv	hh	vv	hh	vv	hh	vv	hh
z_e/h	1.00	0.99	0.01	-0.01	-1.06	-0.96	0.49	0.43
$\lvert S^t/S\rvert$	0.99	0.97	0.02	0.01	0.05	0.05	0.62	0.42
$\lvert S^{gb}/S\rvert$	0.03	0.02	0.99	1.01	0.13	0.08	0.62	0.59
$\lvert S^{gtg}/S\rvert$	0.00	0.00	0.01	0.00	1.10	1.03	0.00	0.00
RCS (dBsm)	8.06	5.19	-0.46	6.16	-6.05	-5.23	-17.2	-15.1

TABLE II
GROUND-TRUTH DATA OF STAND 22

Tree Density :	1142#/Hectare
Tree Height :	8.9 m
Trunk Diameter (DBH) :	14.6 cm
Dry Biomass :	53 (tons/ha)
Needle Length :	10 cm
Needle Diameter :	1.2 mm
Needle Moisture (m_g) :	0.62
Wood Moisture (m_g) :	0.42
Soil Moisture (m_v) :	0.18

III. COMPARISON WITH MEASURED DATA AND SENSITIVITY STUDY

In this section, full simulations of forest stands are carried out. As a first step, the model predictions are compared with the JPL TOPSAR measurements over a selected pine stand, denoted as Stand 22. Then a sensitivity study is conducted to characterize the variations of the scattering phase-center height and correlation coefficient as a function of both forest and INSAR parameters.

Stand 22 is a statistically uniform red pine forest located within Raco Airport, Raco, MI. This scene was selected for this study, because the stand is over a large flat terrain, which reduces the errors in the measured tree height due to possible surface-topographic effects. In addition, the nearby runway provides a reference target at the ground level. Ground-truth data for this stand have been collected since 1991 [24], and careful *in situ* measurements were conducted by the authors during the overflights of TOPSAR in late April 1995. The relevant physical parameters of this stand are summarized in Table II. The vegetation and soil dielectric constants are derived from the measured moisture contents using the empirical models described in [25] and [26].

The JPL TOPSAR is an airborne two-antenna interferometer, operating at C-band (5.3 GHz) with vv-polarization configuration [17]. During this experiment, Stand 22 was imaged twice at two different incidence angles: 39° and 53°. Fig. 6 shows a portion of the 39° radar image, which includes the test stand. Each side of the dark triangle in this image is a runway about 2 mi long. The measured height of the stand is obtained from the elevation difference between the stand and the nearby runway. Using the ground truth reported in Table II, the backscattering coefficient and the location of the scattering phase center as a function of the incidence angle were simulated at 5.3 GHz. As shown in Figs. 7 and 8, excellent agreement between the model predictions and TOPSAR measurements is achieved. The simulated height of the scattering phase center of the same forest for an hh-polarized INSAR having the same antenna configuration and operating at the same frequency, is also shown in Fig. 7. It is shown that the estimated height at the hh-polarization configuration is lower than that obtained from the vv-polarization configuration. This result is usually true for most forest stands, since the ground-trunk backscatter for hh-polarization is much higher than that for vv-polarization. Also noting that the location of the scattering phase center for a ground-trunk backscatter component is at the air–ground interface, the location of the scattering phase center of trees for hh-polarization is lower than that for vv-polarization.

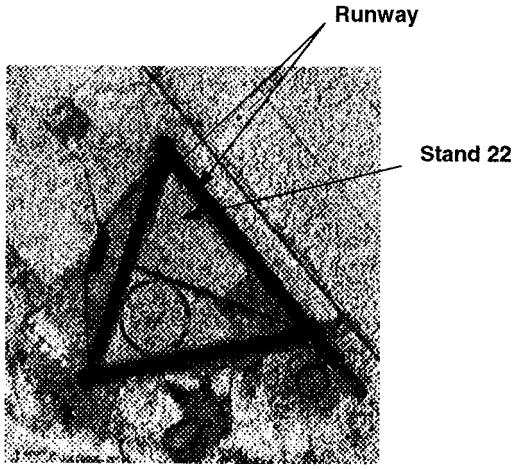

Fig. 6. Portion of a TOPSAR C-band image (σ^0_{vv}), indicating Stand 22 at an airport near Raco, MI.

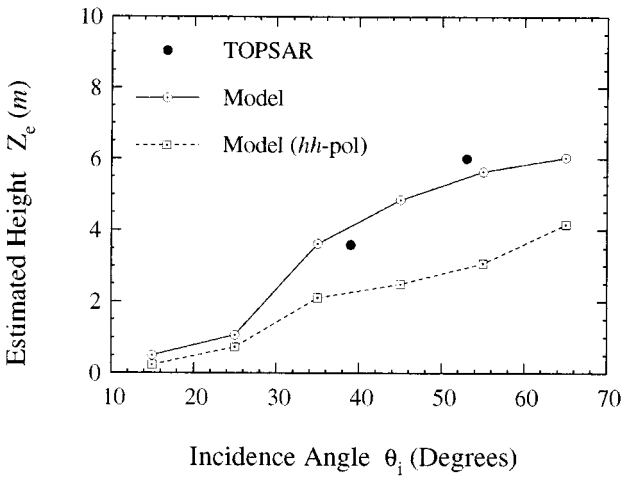

Fig. 7. Estimated height of scattering phase center of Stand 22, compared with the data extracted from two TOPSAR images of the same stand.

The comparison between the simulated σ^0_{vv} and the measured σ^0_{vv} acquired by TOPSAR as a function of the incidence angle is shown in Fig. 8. Also shown in this figure is the contribution of each scattering component (the direct backscatter σ^t and the ground-bounce backscatter σ^{gb}) to the overall backscattering coefficient. It was found that the contribution of the double ground-bounce component σ^{gtg} was relatively small and for most practical cases can be ignored. In this case, at low incidence angles ($\theta_i < 30°$) the ground-bounce backscatter is the dominant component, whereas at higher incidence angles, the direct backscatter becomes the dominant factor. This trend is the cause for the increasing behavior of the scattering phase-center height as a function of the incidence angle found in Fig. 7. It is worth mentioning that the contribution of pine needles to the overall backscattering coefficient was found to be negligible compared

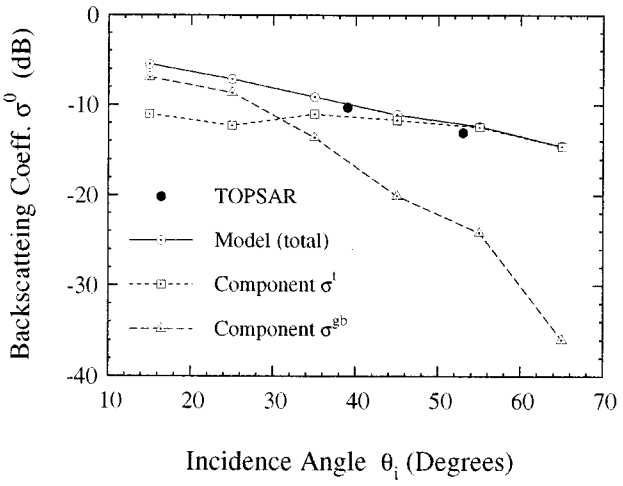

Fig. 8. Simulated backscattering coefficient of Stand 22, compared with the measured σ^0_{vv} extracted from two TOPSAR images of the same stand.

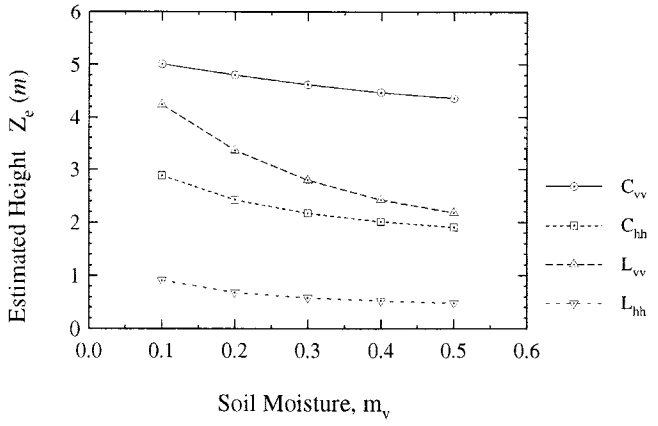

Fig. 9. Estimated scattering phase-center height of Stand 22 as a function of soil moisture, simulated at $\theta_i = 45°$.

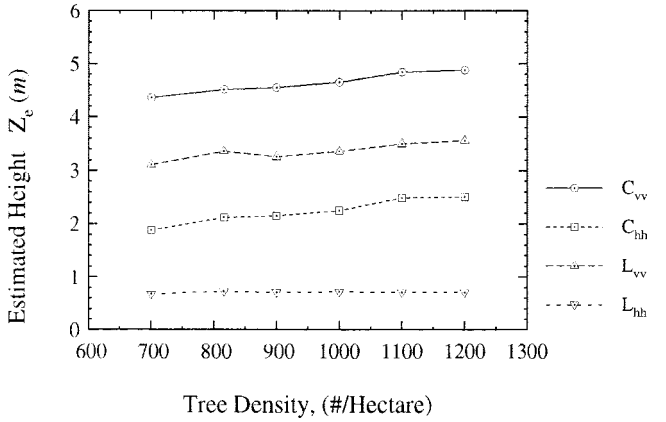

Fig. 10. Estimated scattering phase-center height of Stand 22 as a function of tree density, simulated at $\theta_i = 45°$.

to the contribution from the branches and tree trunks. However, inclusion of the needles in the scattering simulation was necessary because of their significant effect on the extinction.

With some confidence in the scattering model and the algorithm for evaluation of the scattering phase-center height, further simulation can be performed to characterize the dependence of the scattering phase-center height of a forest stand on the system parameters such as frequency, polarization, and incidence angle, and the forest parameters such as tree density, soil moisture, and tree types. In addition, we demonstrate the capability of the present model as a tool for determining an optimum system configuration for retrieving physical parameters of forest canopies. Fig. 9 shows the estimated height of Stand 22 for two principal polarizations at C-band (5.3 GHz) and L-band (1.25 GHz) as a function of the ground's soil moisture, simulated at $\theta_i = 45°$. As the soil moisture increases, the ground-plane reflection will also increase, which in turn causes the ground-bounce scattering component to increase. As a result of this phenomenon, the scattering phase-center height decreases with soil moisture, as shown in Fig. 9. This effect is more pronounced for L-band vv-polarization than other INSAR configurations, suggesting a practical method for monitoring the soil moisture using the apparent height of the forest stand. This high sensitivity at L_{vv} is achieved because of the existence of competitive scattering components. Basically, at low soil moisture, the direct backscatter component is comparable with the ground-bounce component and the scattering phase center lies amidst the canopy. As the soil moisture increases, the ground-bounce scattering component becomes more dominant, which results in lowering the apparent height of the stand. On the other hand, the least sensitive configuration is L_{hh}, since the dominant scattering component, independent of the soil moisture, is the ground-bounce component.

Fig. 10 shows the effect of the tree density on the estimated height of a red pine stand having a similar structure to that of Stand 22 at $\theta_i = 45°$. As the tree density increases, the extinction within the canopy increases, which reduces the ground-bounce component. Increasing the tree density would also increase the direct backscatter component. As a result of these two processes, the apparent height of the canopy increases with increasing tree density, as demonstrated in Fig. 10. As before, the apparent height for L_{hh} configuration does not show any sensitivity to the tree density, indicating that the ground-bounce component remains dominant over the entire simulation range of 700–1200 trees per Hectare. This lack of sensitivity to the apparent height of coniferous stands for L_{hh} suggests that this configuration is most suitable for mapping the surface height of coniferous forest stands.

Now let us examine the response of INSAR when mapping deciduous forest stands. For this study, a red maple stand (Stand 31) is selected, whose structure and scatterers are different from the previous example. A fractal-generated red maple tree and a picture of the stand are shown in Fig. 2. This stand was selected as a test stand to validate the previously developed coherent scattering model [16], using the SIR-C data. The average tree height and tree-number density were measured to be 16.8 m and 1700 trees per Hectare, respectively. Table III provides the detailed

TABLE III
GROUND TRUTH OF STAND 31

Tree Density :	1700/Hectare
Tree Height :	16.8 m
Trunk Diameter (DBH) :	14 cm
Dry Biomass :	140 (tons/ha)
Leaf Density :	382 $\#/m^3$
Leaf Area :	50 $cm^2/\#$
Leaf Thickness :	0.2 mm
Leaf Moisture (m_g) :	0.51
Wood Moisture (m_g) :	0.60
Soil Moisture (m_v) :	0.18

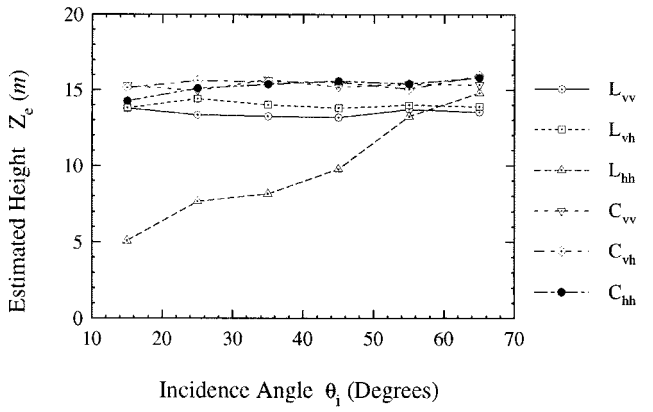

Fig. 11. Estimated scattering phase-center height of Stand 31 as a function of incidence angle, with fully-polarimetric L-Band and C-band response.

ground-truth data from Stand 31. The simulations for estimating the scattering phase-center height are performed fully-polarimetrically at L-band and C-band. Fig. 11 shows the variation of the apparent height of Stand 31 as a function of the incidence angles for co-polarized and cross-polarized L-Band and C-band INSAR configurations. Simulation results at C-band show that except at very low angles of incidence, the scattering phase center is near the top of the canopy. In this case, the backscatter in all three polarizations is dominated by the direct-backscatter components of particles near the canopy top. The same is true for L_{vv} and L_{vh} configurations. However, since penetration depth at L-band is higher than C-band, the location of the scattering phase center appears about 1–3 m below the apparent height at C-band. The scattering phase-center height for L_{hh} configuration, on the other hand, is a strong function of the incidence angle where it appears near the ground surface at low incidence angles and increases to a saturation point near grazing angles. At low incidence angles, the ground-trunk interaction is the dominant scattering mechanism for hh polarization and since the location of the scattering phase for all single ground-bounce terms is on the ground, the overall scattering phase-center height appears close to the ground. Close examination of this figure indicates that a pair of C_{vv} and L_{hh} INSAR data at low incidence angles can be used to estimate the tree height of deciduous forest stands with closed canopies. A C-band foliated canopy behaves

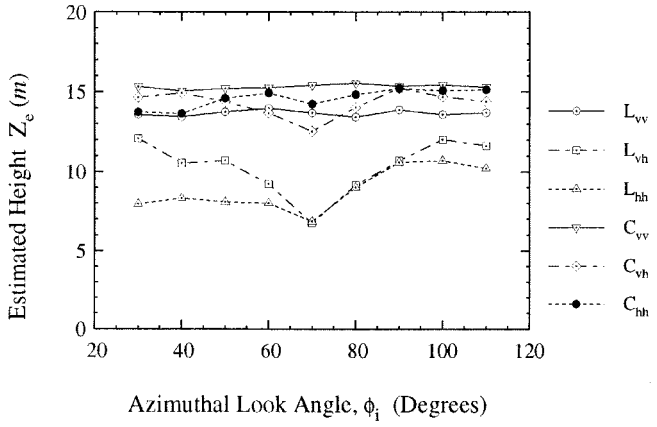

Fig. 12. Estimated scattering phase-center height of Stand 31 over a tilted ground with tilt angle $\theta_g = 10^\circ$ at $\theta_i = 25.4^\circ$.

as a semi-infinite medium, and as shown in [13], the knowledge of extinction would reveal the distance between the location of the scattering phase center and the canopy top (Δd) using $\Delta d = \cos\theta/(2\kappa)$. If an average extinction coefficient (κ) of $0.2N_p$/m is used in the above equation, a distance $\Delta d = 1.77$ m is obtained at $\theta = 45^\circ$. However, a simple relation for evaluating the apparent height for L_{hh} does not exist yet.

Fig. 12 shows the effect of the ground-tilt angle on the estimated scattering phase-center height. This simulation is obtained by setting a ground-tilt angle $\theta_g = 10^\circ$ for a forest stand similar to Stand 31 and calculating the estimated scattering phase-center height as a function of the azimuthal incidence angle ϕ_i at $\theta_i = 25.4^\circ$. As mentioned in [16], there is a strong ground-trunk backscatter around $\phi_i = 70^\circ$, particularly for L_{hh} and L_{vh}. This accounts for the dip in the apparent height simulations for L_{hh} and L_{vh} configurations at $\phi_i = 70^\circ$ shown in Fig. 12.

So far, only the behavior of the mean value of the scattering phase-center height has been investigated. However, the model has the ability to provide an approximate probability-distribution function of the scattering phase-center height. The histograms of the scattering phase-center height can be constructed by recording the simulated results for each scattering simulation. Fig. 13 shows the simulated probability-density function (PDF) of the scattering phase-center height of Stand 22 at $\theta = 45^\circ$ for the three principal polarizations and for both L-Band and C-Band. At L-Band, the scattering phase-center height has a narrow distribution for hh-polarization, indicating that a relatively small number of independent samples are sufficient for estimating the apparent height. At C-band, the scattering phase-center height of the cross-polarized backscatter exhibits a narrower PDF.

As mentioned earlier, the correlation coefficient (α) is an independent parameter provided by INSAR's which, in principle, may be used for inversion and classification processes. The measured correlation coefficient is a function of INSAR parameters such as look angle, baseline distance and angle, radar range to target, and target parameters. To examine the behavior of α as a function of target parameters,

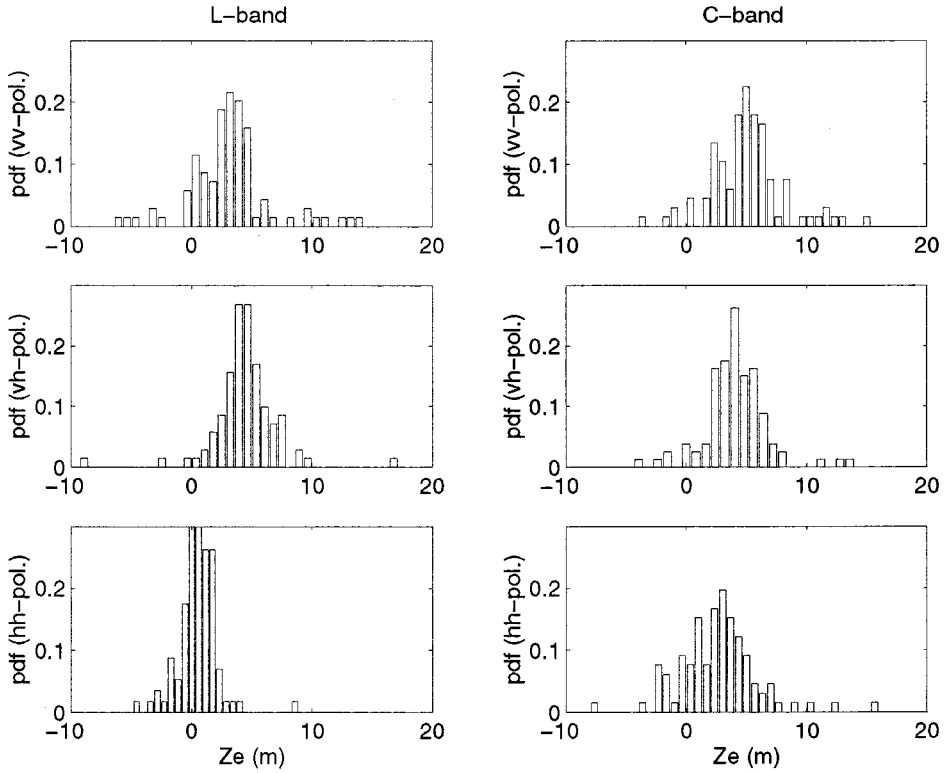

Fig. 13. PDF of the scattering phase-center height of Stand 22 at $\theta_i = 45^\circ$ as a function of frequency and polarization.

the Δk-radar-equivalence relationship given by (7) is used, in which the dependence on INSAR parameters are lumped into one parameter, namely, the frequency shift. Fig. 14 shows the calculated correlation coefficients (α) as a function of the normalized-frequency shift ($\Delta f/f_0$) (corresponding to the baseline distance in an INSAR), simulated for Stand 22 and Stand 31 at $\theta_i = 45°$. As shown in [13], the correlation coefficient is inversely proportional to the width of the PDF (that is, a high value of α indicates a narrow distribution). A comparison between the histograms shown in Fig. 13 and the values of α shown in Fig. 14(a) demonstrates this relationship. It is interesting to note that simulated α for Stand 31 at L_{hh} is significantly smaller than the correlation coefficients at other polarizations [see Fig. 14(b)]. This behavior is a result of the fact that the direct-backscatter and ground-bounce backscatter components are comparable.

It is shown that for the same baseline-to-distance ratio (B/r), which corresponds to a constant $\Delta f/f_0$, α at C-band is smaller than α at L-band independent of polarization. It should be mentioned here that for most practical situations, $\Delta f/f_0$ is of the order of 10—4 or smaller, which renders a value for α near unity ($\alpha > 0.99$). That is, for practical INSAR configurations, the effect of forest parameters on the correlation coefficient appears on the third digit after the decimal point. It can be shown that the measured correlation coefficient is a product of three factors: 1) target decorrelation, which is a function of target parameters only and is proportional to B/r; 2) system decorrelation, which is a function of system slant-range resolution and B/r; and 3) temporal decorrelation, which a function of target change between the two backscatter measurements. Unfortunately, the decorrelation caused by the target is far less than those caused by the other two factors. This puts a serious limitation on the applicability of α for inversion and classification algorithms, since accurate measurement of α with three significant digits is not practical even with two antenna INSAR's. For repeat-pass interferometry, the α values reported for forest stands is below 0.7, which is caused mostly by the temporal decorrelation of the target. Therefore, it does not seem logical to use α as a parameter for classifying forest types. The TOPSAR measured α's for Stand 22 at incidence angles 39° and 53° are, respectively, 0.935 and 0.943, which are below the calculated values of 0.998 and 0.999. This discrepancy can be attributed to processing errors and thermal noise.

IV. Conclusions

In this paper, a scattering model capable of predicting the response of interferometric SAR's when mapping forest stands is described. The model is constructed by combining a first-order scattering model applied to fractal-generated tree structures and a recently developed equivalence relation between an INSAR and a Δk-radar. Using this model, accurate statistics of the scattering phase-center height and the correlation coefficient of forest stands are calculated numerically for the first time. The validity and accuracy of the model are demonstrated by comparing the measured-backscattering coefficient and the

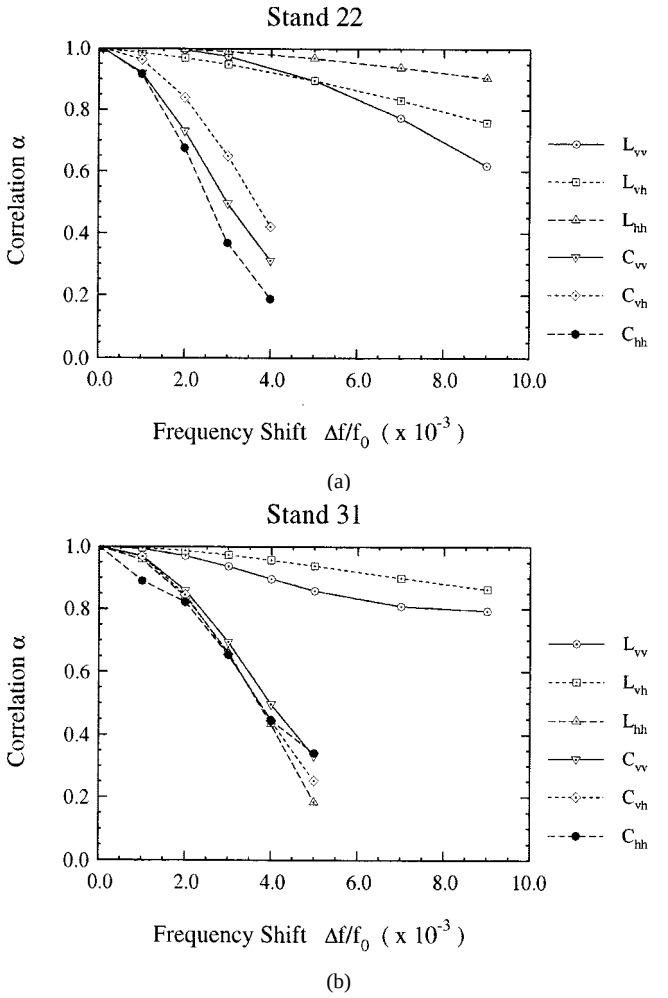

Fig. 14. Correlation coefficient as a function of the frequency shift, simulated from (a) Stand 22 and (b) Stand 31.

scattering phase-center height of a test stand with those calculated by the model. Then an extensive sensitivity analysis is carried out to characterize the dependence of the scattering phase-center height on forest physical parameters such as soil moisture, tree density, and tree types, and INSAR parameters such as frequency, polarization, and incidence angle. The ability of the model to predict the PDF of the scattering phase-center height and the correlation coefficient is also demonstrated. It is shown that for practical INSAR configurations, the correlation coefficient of forest stands is near unity, much larger than what can be measured by existing INSAR systems.

ACKNOWLEDGMENT

The authors would like to thank the JPL Radar Science Group for their help in providing the TOPSAR image data used in this study.

REFERENCES

[1] F. T. Ulaby, K. Sarabandi, K. MacDonald, M. Whitt, and M. C. Dobson, "Michigan microwave canopy scattering model," *Int. J. Remote Sens.*, vol. 11, no. 7, pp. 1223–1253, 1990.

[2] L. Tsang, C. H. Chan, J. A. Kong, and J. Joseph, "Polarimetric signature of a canopy of dielectric cylinders based on first and second order vector radiative transfer theory," *J. Electromagn. Waves Applicat.*, vol. 6, no. 1, pp. 19–51, 1992.

[3] M. A. Karam, A. K. Fung, R. H. Lang, and N. H. Chauhan, "A microwave scattering model for layered vegetation," *IEEE Trans. Geosci. Remote Sensing*, vol. 30, pp. 767–784, July 1992.

[4] K. Sarabandi, "Electromagnetic scattering from vegetation canopies," Ph.D. dissertation, Univ. Michigan, Ann Arbor, 1989.

[5] G. Sun and K. J. Ranson, "A three-dimensional radar backscatter model of forest canopies," *IEEE Trans. Geosci. Remote Sensing*, vol. 33, pp. 372–382, Mar. 1995.

[6] K. C. McDonald and F. T. Ulaby, "Radiative transfer modeling of discontinuous tree canopies at microwave frequencies," *Int. J. Remote Sensing*, vol. 14, no. 11, 1993.

[7] J. B. Cimino, C. Elachi, and M. Settle, "SIR-B the second shuttle image radar experiment," *IEEE Trans. Geosci. Remote Sensing*, vol. 24, pp. 445–452, July 1986.

[8] R. L. Jordan, B. L. Huneycutt, and M. Werner, "The SIR-C/X-SAR synthetic aperture radar system," *IEEE Trans. Geosci, Remote Sensing*, vol. 33, pp. 829–839, July 1996.

[9] E. Rodriguez and J. M. Martin, "Theory and design of interferometric synthetic aperture radars," *IEEE Proc.*, vol. F39, no. 2, pp. 147–159, 1992.

[10] J. O. Hagberg, L. M. H. Ulander, and J. Askne, "Repeat-pass SAR interferometry over forested terrain," *IEEE Trans. Geosci. Remote Sensing*, vol. 33, pp. 331–340, Mar. 1995.

[11] U. Wegmuller and C. L. Werner, "SAR interferometry signature of forest," *IEEE Trans. Geosci. Remote Sensing*, vol. 33, pp. 1153–1161, Sept. 1995.

[12] N. P. Faller and E. H. Meier, "First results with the airborne single-pass DO-SAR interferometer," *IEEE Trans. Geosci. Remote Sensing*, vol. 33, pp. 1230–1237, Sept. 1995.

[13] K. Sarabandi, "Δk-radar equivalent of interferometric SAR's: A theoretical study for determination of vegetation height," *IEEE Trans. Geosci. Remote Sensing*, vol. 35, pp. 1267–1276, Sept. 1997.

[14] R. N. Treuhaft, S. N. Madsen, M. Moghaddam, and J. J. van Zyl, "Vegetation characteristics and underlying topography from interferometric radar," *Radio Sci.*, vol. 31, no. 6, pp. 1449–1485, 1996.

[15] J. I. H. Asken, P. B. G. Dammert, L. M. H. Ulander, and G. Smith, "C-band repeat-pass interferometric SAR observations of the forest," *IEEE Trans. Geosci. Remote Sensing*, vol. 35, pp. 25–35, Jan. 1997.

[16] Y. C. Lin and K. Sarabandi, "A Monte Carlo coherent scattering model for forest canopies using fractal generated trees," *IEEE Trans. Geosci. Remote Sensing*, vol. 37, pp. 36–40, Jan. 1997.

[17] H. A. Zebker, S. N. Madsen, J. Martin, K. B. Wheeler, T. Miller, Y. Lou, G. Alberti, S. Vetrella, and A. Cucci, "The TOPSAR interferometric radar topographic mapping instrument," *IEEE Trans. Geosci. Remote Sensing*, vol. 30, pp. 933–940, Sept. 1992.

[18] B. Mandelbrot, *Fractal Geometry of Nature*. New York: W. H. Freeman, 1983.

[19] C. C. Borel and R. E. McIntosh, "A backscattering model for various foliated deciduous tree types at millimeter wavelengths," in *Proc. IGARSS'86*, Zürich, Switzerland, 1986, pp. 867–872.

[20] P. Prusinkiewicz and A. Lindenmayer, *The Algorithmic Beauty of Plants*. New York: Spring-Verlag, 1990.

[21] Y. C. Lin and K. Sarabandi, "Electromagnetic scattering model for a tree trunk above a tilted ground plane," *IEEE Trans. Geosci. Remote Sensing*, vol. 33, pp. 1063–1070, July 1995.

[22] K. Sarabandi and T. B. A. Senior, "Low-frequency scattering from cylindrical structures at oblique incidence," *IEEE Trans. Geosci. Remote Sensing*, vol. 28, pp. 879–885, Sept. 1990.

[23] Y. C. Lin, "A fractal-based coherent microwave scattering model for forest canopies," Ph.D. dissertation, Univ. Michigan, Ann Arbor, 1997.

[24] K. M. Bergen, M. C. Dobson, T. L. Sharik, and I. Brodie, "Structure, composition, and above-ground biomass of SIR-C/X-SAR and ERS-1 forest test stands 1991-1994, Raco MI Site," Univ. Mich. Radiation Lab., Ann Arbor, Tech. Rep. 026511-7-T, 1995.

[25] M. T. Hallikainen, F. T. Ulaby, M. C. Dobson, M. A. El-Rayes, and L.-K. Wu, "Microwave dielectric behavior of wet soil—Part I: Empirical models and experimental observations," *IEEE Trans. Geosci. Remote Sensing*, vol. GE-23, pp. 25–34, Jan. 1985.

[26] F. T. Ulaby and M. A. Elrayes, "Microwave dielectric spectrum of vegetation—Part II: Dual-dispersion model," *IEEE Trans. Geosci. Remote Sensing*, vol. GE-25, pp. 550–557, Sept., 1987.

Kamal Sarabandi (S'87–M'90–SM'93–F'00) received the B.S. degree in electrical engineering from Sharif University of Technology, Tehran, Iran, in 1980 and the M.S.E. degree in electrical engineering, the M.S. degree in mathematics, and the Ph.D. degree in electrical engineering, in 1984, 1989, and 1989, respectively, from the University of Michigan, Ann Arbor.

From 1980 to 1984, he worked as a Microwave Engineer in the Telecommunication Research Center, Iran. He is presently an Associate Professor in the Department of Electrical Engineering and Computer Science, University of Michigan. He has 18 years of experience with microwave sensors and radar systems. In the past eight years, he has served as the Principal Investigator and Co-Investigator on many projects sponsored by NASA, JPL, ARO, ONR, ARL, and GM all related in one way or the other to microwave and millimeter wave radar remote sensing. He has published many book chapters and more than 80 papers in refereed journals on electromagnetic scattering, random media modeling, microwave measurement techniques, radar calibration, application of neural networks in inverse scattering problems, and microwave sensors. He has also had more than 140 papers and invited presentations in national and international conferences and symposia on similar subjects.

Dr. Sarabandi is listed in *American Men & Women of Science* and *Who's Who in Electromagnetics*. He has been a member of the IEEE GEOSCIENCE AND REMOTE SENSING AdCom since January 1998 and has served as the Chairman of the Geoscience and Remote Sensing Society, Southeastern Michigan chapter, from 1992 to 1998. He is also a member of Commission F of URSI and of The Electromagnetic Academy. He was a recipient of the 1996 Teaching Excellence Award, the 1997 Henry Russel Award from the Regent of The University of Michigan, and the 1999 GAAC Distinguished Lecturer Award from the German Federal Ministry for Education, Science, and Technology.

Yi-Cheng Lin (S'92–M'98) received the B.S. degree in nuclear engineering from National Tsing-Hua University, Hsinchu, Taiwan, R.O.C., in 1987, the M.S. degree in electrical engineering from National Taiwan University, Taipei, in 1989, and the Ph.D. degree in electrical engineering from the University of Michigan, Ann Arbor, in 1997.

He is currently a Senior Engineer at Qualcomm, Inc., San Diego, CA, where he has been working in the antenna group of the global satellite communication systems (Globalstar). His research interests include electromagnetic modeling of scattering problems, microwave remote sensing, near-field measurements, and dielectric resonator antennas.